Synchrotron Small Angle X-ray Scattering Study of Crystalline Structures and Isothermal Crystallization Kinetics of Poly(aryl ether ether ketones)

Jian Wang,[†] Marta Alvarez,[†,‡] Wanjin Zhang,[§] Zhongwen Wu,[§] Yingjie Li,[†] and Benjamin Chu*[,∥,⊥]

Chemistry Department, State University of New York at Stony Brook, Stony Brook, Long Island, New York 11794-3400, Chemistry Department, Jilin University, Changchun, Jilin 130023, People's Republic of China, and Max-Planck-Institut für Polymerforschung, D-6500 Mainz, Germany

Received May 18, 1992; Revised Manuscript Received August 31, 1992

ABSTRACT: Time-resolved synchrotron small angle X-ray scattering (SAXS) was employed to investigate crystallization behaviors at elevated temperatures and fast isothermal crystallization kinetics around ~230 °C for poly(aryl ether ether ketones) (PEEKs). The crystalline structure parameters were evaluated by means of one-dimensional correlation function analysis. The long period, the lamellar thickness, and the one-dimensional crystallinity as a function of temperature were compared between two samples which had different repeat units in the polymer backbone. For two samples, the long period and the lamellar thickness were found to increase with increasing crystallization temperature simultaneously. For the crystallization kinetics study, the initial nonisothermal condition due to the temperature retardation in samples was corrected using a multistep T-jump process. A single exponential behavior of the invariant change during isothermal crystallization was observed and interpreted by the diffusion-controlled mechanism. The activation energies of the segmental diffusion were estimated from the data under the nonisothermal condition. The crystallization rates were compared between two samples.

Introduction

Poly(aryl ether ether ketone) (PEEK) is a semicrystalline thermoplastic polymer which usually has a melting point (T_m) of above 330 °C and a glass transition temperature (T_g) of around 140 °C depending on the thermal history. Both T_m and T_g for PEEK are claimed to be highest in crystalline polymers. PEEK has found a variety of applications in advanced composites[1-5] becuase of its high thermal stability, good chemical resistance, and excellent electrical and mechanical properties. During the last decade, a remarkable number of publications concerning the crystalline structures and physical properties of PEEK has emerged in the literature.[6] Wide angle X-ray diffraction measurements[7-16] have revealed the crystalline unit cell dimension to be ~10 Å along the polymer chain direction and the maximum achievable crystallinity to be ~40%. Differential scanning calorimetry (DSC) traces of crystallized PEEK[17-39] exhibit two distinct melting endotherms. The explanations for the double-melting behavior can be grouped into two categories.[24] The double endotherms are associated with (1) two distinct morphologies and (2) partial melting and recrystallization of one initial crystal morphology with a characteristic of crystallization history. By using electron microscopy in combination with an itching technique, some authors[28] have reached the conclusion that the high melting lamellae are formed prior to the lower melting lamellae that lay between the primary lamellae in support of the two-morphology hypothesis. Investigation of spherulite growth of PEEK by microscopy has also been reported.[40-42]

As a result of high T_m and of fast crystallization kinetics, the processing control for PEEK is often difficult in many industrial applications. A promising approach toward reducing the processing temperature and the crystallization rate is being explored by some of the authors[43] by using copolymers which involve the introduction of more rigid monomer units of diphenol into the PEEK backbone. It has been found[43] that the T_m first decreases with an increase in the diphenol composition in PEEK and then, above an onset point, increases with a further increase in the diphenol composition. For example, T_m = 295 and 385 °C at a diphenol composition of 30% and 70%, respectively. Besides, the T_g of PEEK is increased monotonically with increasing diphenol composition, which is of significant importance because the modulus of elasticity is considerably reduced near the glass transition temperature. For example, direct application in magnet wire coating materials used in nuclear reactor and aerospace industries, the modified PEEK with diphenol units in its backbone having lower T_m values and lower crystallization rates meets the processing requirements.

The aim of the present study is 2-fold. First, we examine the hypotheses on the double melting behavior of PEEK based on the experimental data of small angle X-ray scattering (SAXS), which has seldomly been employed for PEEK studies.[44] Second, we investigate the effect of the diphenol unit, which has been incorporated into the PEEK backbone, on crystalline structures and the fast crystallization kinetics from the glassy state by performing time-resolved SAXS measurements on a regular PEEK and a modified PEEK with 30% diphenol unit. The crystalline structure parameters and the crystallization rate will be evaluated by using an electron density correlation function analysis and a generalized diffusion model, respectively.

* To whom all correspondence should be addressed (use Chemistry Department address).
† Chemistry Department, State University of New York at Stony Brook.
‡ Permanent address: Instituto de Estructura de la Materia, CSIC, Serrano 123, Madrid-28006, Spain.
§ Chemistry Department, Jilin University.
∥ Max-Planck-Institut für Polymerforschung.
⊥ On leave from: Department of Chemistry, State University of New York at Stony Brook, Stony Brook, Long Island, New York 11794-3400.

0024-9297/92/2225-6943$03.00/0

Experimental Section

Materials. The PEEKs used in our study have the following structural formulas:

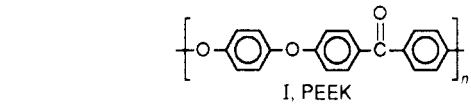

I, PEEK

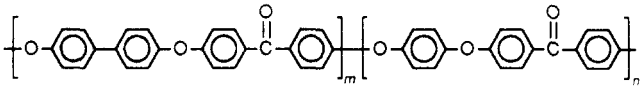

II, D-PEEK

The samples of structure I and of structure II are denoted as, respectively, PEEK and D-PEEK throughout this paper. The samples were prepared via polycondensation of bis(4-fluorophenyl) ketone with hydroquinione for PEEK or with a mixture of hydroquinione/diphenol (=70:30 by mole) for D-PEEK according to the method described in ref 4. The weight-average molecular weight for PEEK and D-PEEK was estimated to be, respectively, 6.1×10^4 and 5.0×10^4 g/mol.[4] D-PEEK is a random copolymer with a composition of 30 mol % diphenyl unit. Amorphous sample films of 0.5-mm thickness were melt compression-molded at 380 °C for 10 min (under a pressure of 100 kg/cm^2) and quenched into ice water. The same amorphous structure could be achieved if the sample were quenched into liquid nitrogen. The samples were dried in a vacuum oven below 60 °C for 2 weeks and then kept in a desiccator. Disk-shaped samples of 8 mm in diameter were cut from the molded films and fitted into the sample cell.

Small Angle X-ray Scattering. SAXS experiments were performed at the X3A2 State University of New York (SUNY) Beam Line, National Synchrotron Light Source (NSLS), Brookhaven National Laboratory (BNL). A modified Kratky camera[45] and a linear photodiode array position-sensitive detector[46] operated with an OMA controller (EG&G, PARC, Model 1453) were used to collect scattered X-ray photons. The detector had a channel-to-channel distance of 25 μm and a usable window length of 25 mm. Two ionization chambers were placed before and after the sample holder to monitor the incident and the transmitted beam intensity, respectively. A tantalum beam stop with a sharp edge was used to minimize the parasitic scattering. The sample-to-detector distance was 495 mm, covering a scattering vector q ($=(4\pi/\lambda)\sin(\theta/2)$ with θ being the scattering angle and the wavelength $\lambda = 0.154$ nm) from 0.1 to 2 nm^{-1}. The SAXS patterns were corrected for sample thickness, sample absorption, background, beam intensity decay, detector uniformity, and thermal density fluctuations.

Temperature jump from one level to another was accomplished by using a dual-chambered temperature-jump device covering a temperature range from room temperature to 450 °C with an average fluctuation of ±1 °C.

SAXS Data Analysis

Intensity Distribution and Correlation Function. SAXS reflects electron density fluctuations within a sample over a length range larger than the usual interatomic distances. For a two-phase system consisting of crystalline domains and an amorphous matrix, a SAXS profile, or its corresponding correlation function after Fourier transformation, provides the information about the mean distance of the centers of gravity of two adjacent lamellae, namely the long period L, the average lamellar dimension, the thickness of the interface and, if the absolute scattered intensity is known, the electron density difference between the crystalline and the amorphous regions. The SAXS intensity distribution in q space is given by a Fourier transform of the correlation function of the electron density fluctuations[47]

$$I_v(q) = V\int_0^\infty 4\pi r^2 \gamma(r) \frac{\sin(qr)}{qr} dr \quad (1)$$

where r ($=|r_1 - r_2|$) is the relative distance for every pair of points and V is the scattering volume illuminated by the incident beam. The correlation function $\gamma(r)$ is defined by

$$\gamma(r) = \langle(\rho(r_1) - \bar{\rho})\,(\rho(r_2) - \bar{\rho})\rangle \quad (2)$$

with $\rho(r_i)$ and $\bar{\rho}$ being the electron density at point of r_i and the mean value, respectively. The correlation function can be obtained by performing the standard inverse Fourier transform of eq 1. For unoriented samples of partially crystalline polymers, if the stacks of aparallel lamellae are isotropically distributed and densely packed, the system can be described by a one-dimentional correlation function of the electron density fluctuations which are measured along the direction perpendicular to the inner surface of a stack and passing through amorphous regions.[48] The normalized one-dimensional correlation function, which is related to the observed scattered intensity in a relative scale, $I(q)$, by its value at zero distance is given by

$$\gamma_1(z) = \frac{1}{\gamma_1(0)}\int_0^\infty q^2 I(q)\cos(qz)\,dq \quad (3)$$

where z is the coordinate along which the electron density distribution is measured. An appropriate smoothing approach is often required to improve the signal-to-noise ratio before applying eq 3 to an experimental curve. In addition, it is also necessary to extend data points at both lower and higher q values. The data points of the scattered intensity could be extended to zero q by using a model such as the Debye–Bueche model[49,50]

$$I(q) = \frac{A}{(1 + \xi^2 q^2)^2} \quad (4)$$

where A is a constant and ξ an inhomogeneity length. Similarly, the data points at large q values could be damped to infinite q value (where $I(q) \to 0$) by using the modified Porod model[51]

$$I(q) = K_p \frac{\exp(-\sigma^2 q^2)}{q^4} \quad (5)$$

where K_p is the Porod constant and σ the standard deviation of a Gaussian smoothing function.

Invariant. The invariant is defined as an integral of the scattered intensity after Lorentz correction over q[47]

$$Q = \int_0^\infty q^2 I(q)\,dq \quad (6)$$

For an ideal two-phase system with a well-defined interface, the invariant per unit scattering volume can be expressed as

$$Q = \Delta\rho^2 \phi (1 - \phi) \quad (7)$$

where ϕ is the volume fraction of one of the two phases and $\Delta\rho$ ($=\rho_1 - \rho_2$) is the difference in the electron density of the two phases. Qualitatively, if $\Delta\rho$ remains unchanged, the invariant will increase monotonically with an increase in the volume fraction of the phase-separated domains when ϕ is below 0.5.

Thermal Density Fluctuations and Interface Thickness. The thermal density fluctuations constitute a background scattering and must be substracted from SAXS profiles before any calculations. Ruland[51] suggested a method on the basis of the Porod law to determine the thermal density fluctuations and the interface thickenss

$$I(q)\,q^4 = K_p H^2(q) + I_{fl} q^4 \quad (8)$$

where $H^2(q) = \exp(-\sigma^2 q^2)$ is a Gaussian smoothing function which accounts for the negative deviations from the Porod

law due to the interface with σ being the standard deviation which is associated with the interface thickness E by the relation $E = (12)^{1/2}\sigma$, and I_{fl} is the scattering background due to the thermal density fluctuations. I_{fl} can be estimated from the slope of a plot of $q^4I(q)$ versus q^4. Plotting $\ln\{[I(q) - I_{fl}]q^4\}$ versus q^2 allows for an estimation of σ and thus of the interface thickness.

Results and Discussion

A. Crystalline Morphology. The chemical structure of D-PEEK differs from that of PEEK only in the monomer unit of the phenyl rings between two oxygen atoms; i.e., the single phenyl rings are partially replaced by diphenyl rings in D-PEEK. This variation of molecular structure increases, on the one hand, the T_g by ~10 °C because of the higher rigidity of diphenyl rings and decreases, on the other hand, the maximum crystallinity by ~20% due to the reduction in the chain regularity. SAXS patterns were undertaken for PEEK and D-PEEK after the amorphous samples, without crystallization thermal history, were quickly heated up to each temperature and thermally equilibrated for 15–20 min to allow the sample to reach thermal equilibrium and to crystallize, noting that the high viscosity at low temperatures could prevent the sample from achieving complete crystallization over a short time period. Figure 1 shows the SAXS profiles of PEEK and of D-PEEK at temperatures ranged from room temperature to 360 °C. The patterns for both PEEK and D-PEEK below ~170 °C show only simple decay curves which are indicative of amorphous morphology without an appreciable amount of the crystalline phase. As the temperature is raised above ~170 °C, a maximum at $q \sim 0.4$ nm^{-1} is present. The maximum shows an increase in its magnitude with increasing temperature and finally disappears at temperatures higher than around 330 °C for PEEK (refer to T_m = 334 °C from DSC) and around 300 °C for D-PEEK (refer to T_m = 295 °C from DSC). It is evident that the maximum in the SAXS profiles is very sensitive to the formation and the destruction of crystalline structures. From the lower T_m values, the lamellar thickness for D-PEEK could be expected to be smaller than that for PEEK.

Most data analysis of SAXS profiles does not require an absolute value of the scattered intensity. Therefore, no attempt was made to place the experimentally obtained quantities associated with the scattered intensity to an absolute scale. A direct comparison of the invariant between PEEK and D-PEEK is shown in Figure 2 as a function of temperature. The invariant rises rapidly from a stable value at around 130 °C for PEEK and around 170 °C for D-PEEK, denoting a lower limit of crystallization temperature, T_c, for the primary crystallization. The Q values then increase monotonically with temperature below ~330 °C for PEEK and below ~260 °C for D-PEEK and finally drop down to a value comparable to the initial one. The increased lower-T_c-limit and decreased T_m for D-PEEK are consistent with the fact that the rigid diphenyl ring in D-PEEK has a more restricted mobility when compared with the single phenyl ring in PEEK and is more difficult to fit into a unit cell. If we assume that the electron density difference between the crystalline and the amorphous phases for D-PEEK to be roughly the same as for PEEK, the reduction in the crystallinity is then mainly responsible for the decrease in the invariant. The ratio of the maximum invariant for D-PEEK over that for PEEK is about 0.4, which is comparable to the maximum crystallinity ratio of D-PEEK to PEEK as determined from density measurements (see Table I). It should be noted that the difference in the electron density between the crystalline and the amorphous phases might not remain constant with temperature due to the difference in the thermal expansions of the crystalline and the amorphous

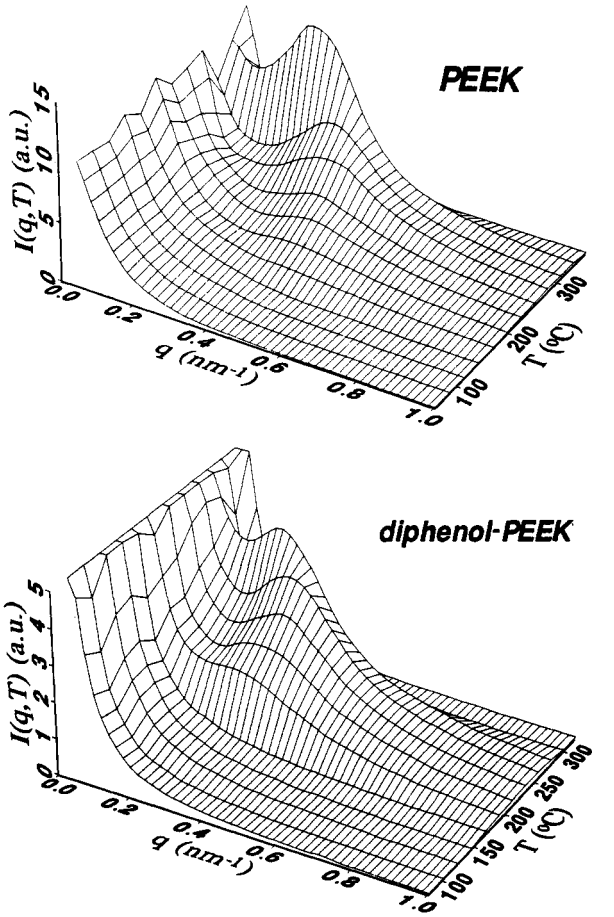

Figure 1. SAXS profiles for crystallized (a, top) PEEK and (b, bottom) D-PEEK at elevated temperatures from the amorphous state. The amorphous samples were thermally equilibrated for 15–20 min at each temperature before measurements were taken in order to allow the sample to reach thermal equilibrium and to crystallize. Each SAXS profile was accumulated for 200 s and was smoothed firstly by adding up 10 points together for a better signal-to-noise ratio of the scattered intensity at an expense of the q resolution and secondly by using a cubic spline smoothing method. An obvious peak related to the long period of the lamellar structure started to show up at $q \sim 0.4$ nm^{-1} above ~170 °C and disappeared above ~330 °C for PEEK and ~300 °C for D-PEEK. For a clear view of the maximum, the data points of the SAXS profiles at both small and large q values are not presented.

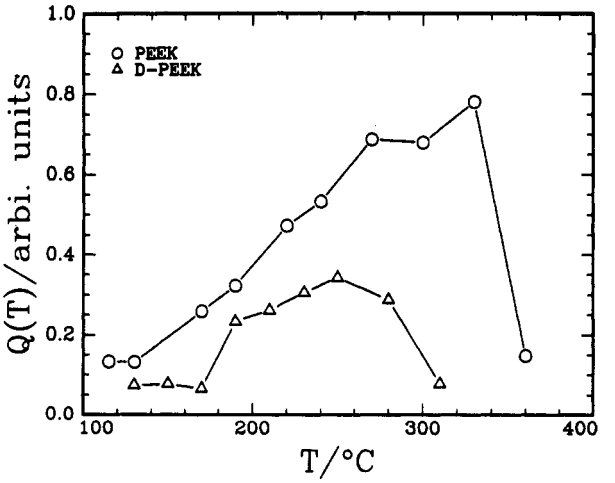

Figure 2. SAXS invariant as a function of temperature for PEEK and D-PEEK.

Table I
Crystalline Structure Parameters[d] at Different Temperatures

T (°C)	L (nm)	d (nm)	f_c	l_a/d^a	E^b (nm)	X_c^c
			PEEK			
170	10.1	2.30	0.228	3.39	0.42	0.221
190	10.9	2.80	0.257	2.89	0.39	0.280
220	11.0	2.99	0.272	2.68	0.22	0.332
240	11.9	3.30	0.277	2.61	0.26	0.359
270	12.6	3.43	0.272	2.67	(0.45)	0.370
300	13.7	3.74	0.273	2.66	0.23	0.391
330	16.9	5.00	0.296	2.38	0.42	0.420
			D-PEEK			
170						
190	14.6	2.31	0.158	5.32	0.71	0.154
210	14.6	2.50	0.171	4.84	0.54	0.217
230	14.5	3.05	0.210	3.77	0.34	0.222
250	15.0	3.30	0.220	3.55	0.69	0.224
280	17.8	3.71	0.208	3.80	0.62	0.227
310						

[a] $l_a/d = (L - d)/d$. [b] E is the interface thickness determined according to eq 8. The value in the bracket is exceptionally off the tendency of the temperature dependence. [c] X_c is overall crystallinity determined by density measurements. [d] Precision for the values is of the order of two significant figures.

regions. The change in electron density difference at different temperatures may more or less contribute to the increase in the invariant at elevated temperatures but must be of secondary importance because the change in crystallinity should pronouncedly dominate the scattering power.

Figure 3 shows the normalized one-dimensional correlation functions at different temperatures for (a) PEEK and (b) D-PEEK. The normalized correlation function $\gamma_1(z)$ shows a unit value at $z = 0$ and a minimum and a maximum typical of two-phase systems. The positions of the minimum and of the maximum vary distinctly with temperature. An evaluation of the shape and the nature of these correlation functions was carried out following the method reported in refs 52–54 in which various parameters regarding the crystalline structures were deduced from the shape of the one-dimensional correlation functions for polyethylene and for poly(ethylene terephthalate) (PET) on the basis of a planar and parallel lamellar model. In the present work, we are mainly concerned about the long period, L, the lamellar thickness, d, the amorphous thickness, l_a, as well as the crystallinity. A typical analysis of the correlation function shape for PEEK at 240 °C is demonstrated in Figure 4. The long period can be determined from the position of the first maximum in the correlation function. In the initial slope region, called the "self-correlation region", the curve shape accounts for the dimensions of the lamellae and the interface. The $\gamma_1(z)$ should decrease linearly to its bottom line, called the "base line" which is a horizontally extended line from the visible flattened bottom of the first minimum at a characteristic point $z=d$. This "base line", however, cannot be easily identified for most systems as the flattened bottom of the first minimum is often distorted by the broad size distribution of the lamellae and the interface as well as the heterogeneities in the structure. However, the "base line" could be estimated from the density data[53]

$$B = \frac{(\langle\rho\rangle - \langle\rho_a\rangle)^2}{Q} = -\frac{X_c}{1 - X_c} \tag{9}$$

where B is the negative coordinate of the "base line" for a normalized one-dimensional correlation function and the subscript a denotes amorphous structure and X_c is the overall crystallinity. The unknown "base line" can thus be estimated from the density or crystallinity data. The lamellar thickness was estimated from the position of the intercept of a continuation of the linear section of the initial slope with the "base line". In this model, the one-dimensional crystallinity is defined as $f_c = d/L$ and the amorphous thickness $l_a = (1 - f_c)L$. Table I lists the lamellar structure parameters estimated from the corre-

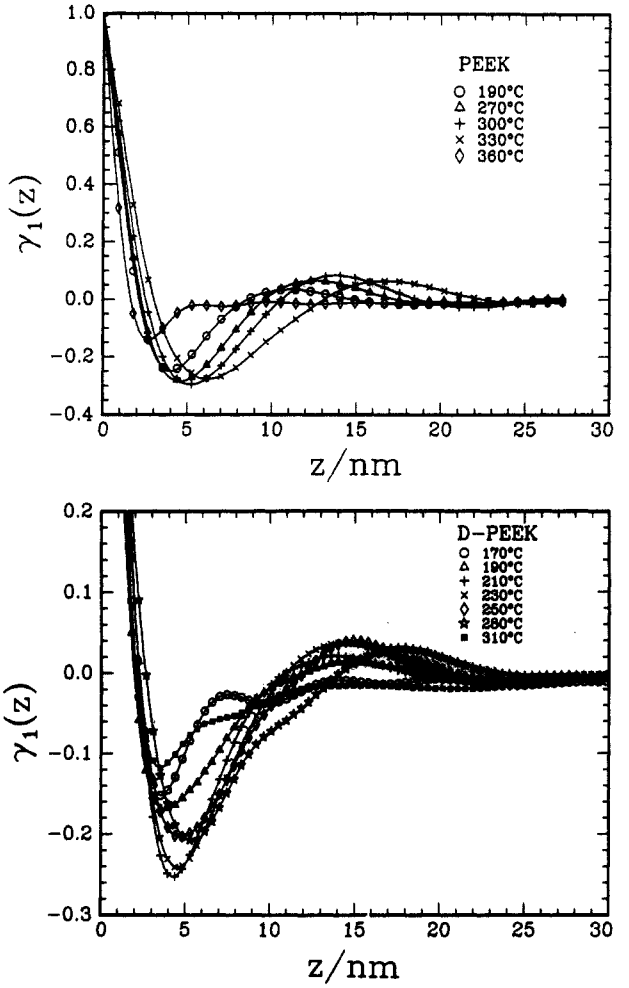

Figure 3. Normalized one-dimensional correlation functions of electron density fluctuations at elevated temperatures: (a, top) PEEK; (b, bottom) D-PEEK. The position of the maxima in each curve characterizes the long period denoting the most probable interdomain spacing.

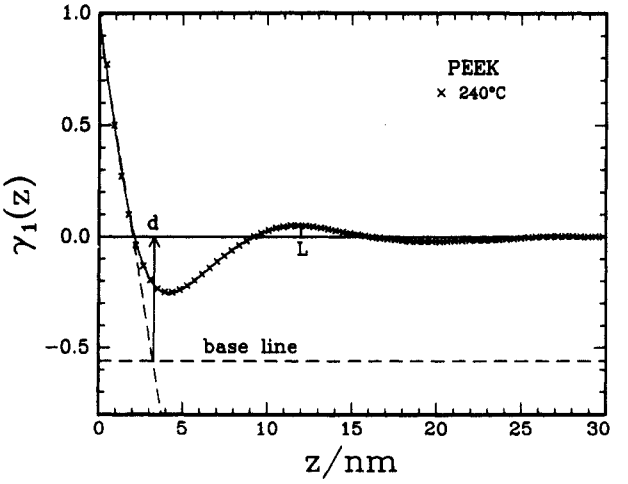

Figure 4. Typical shape analysis of the one-dimensional correlation function of electron density fluctuations for PEEK at 240 °C. The long period and the lamellar thickness are indicated on the abscissa. The base line coordinate was calculated using eq 9.

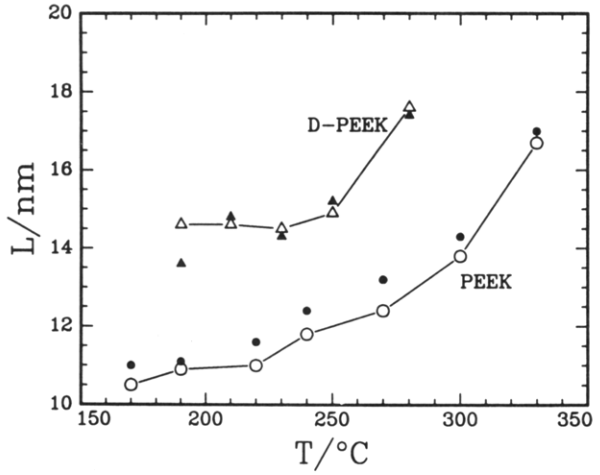

Figure 5. Temperature dependence of the long period of lamellar structure for PEEK and D-PEEK. Open symbols represent the values determined from the correlation functions while the solid symbols represent the values estimated by applying the Bragg equation to the scattered intensity maximum after Lorentz correction.

lation function analysis using the above described method. As all the values listed in Table I are self-consistent in our study, a comparison between different temperatures and between different samples was made in order to elucidate the structure effect on the crystallization behavior. The long period is plotted against temperature in Figure 5 for a direct comparison. The open symbols denote the long periods obtained from the correlation function analysis and the solid symbols denote the ones from the Lorentz corrected SAXS profiles by applying the Bragg equation to the maximum. A satisfactory agreement between the two methods implies that the one-dimensional correlation function is suitable to describe our semicrystalline polymers.

One can note from Table I that D-PEEK demonstrates a substantially larger long period, a smaller lamellar thickness, and a lower crystallinity as compared to those for PEEK over a wide temperature range. This is in agreement with the invariant analysis and is therefore more evidence for the reduced crystallinity for D-PEEK. As can be seen again from Table I, the ratio of the amorphous layer thickness to the lamellar thickness for D-PEEK is about 1.4–1.9 times as large as that for PEEK over the temperature range we studied. It has been suggested that PEEK adopts a folded-chain conformation in the lamellar structure as in the cases for most other semicrystalline polymers.[8] The distance between the two adjacent oxygens in D-PEEK is twice that in PEEK. Therefore, more monomer units should be required for the D-PEEK chains to fold, and thus a larger amorphous layer thickness could be expected. For both PEEK and D-PEEK, the long period and the lamellar thickness as well as the crystallinity increase with increasing temperature below the melting point. The above evidence seems to be strongly in favor of the proposed two-morphology supposition based on the DSC measurements, as shown schematically in Figure 6, that at high temperatures the low melting lamellae which lay between the primary lamellae[28] may experience a melting and recrystallization and eventually merge into the primary lamellae.[21]

The interface thickness, E, was estimated from a Porod plot according to eq 8 and was listed in Table I. In principle this parameter can also be estimated from the correlation function analysis.[53] The initial curvature in the correlation function at q below the first minimum position (see Figure

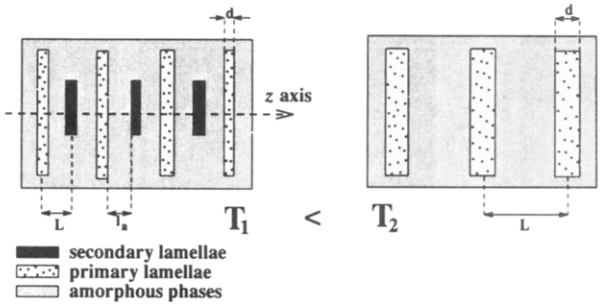

Figure 6. Schematic representation of lamellar morphology: L, long period; l_a, amorphous thickness; d, lamellar thickness. T_1 and T_2 represent two temperature values which are between the lower-limit crystallization temperature and the melting point.

4) contains the information on the interface thickness. However, in our case it was difficult to locate precisely the transition point as a result of a continuous concave-upward curvature in the very beginning of the correlation function. Roughly from the correlation function analysis, the interface thickness was on the order of ≈1 nm, which was much lower than expected in view of the high melting point and molecular rigidity of PEEK. In any case, it was possible for us to make a relative comparison between PEEK and D-PEEK if we chose the same approach to estimate the interface thickness. From Table I we can see that the D-PEEK value is roughly 50% larger than that for PEEK. This result could be explained by a perturbation of the crystallization from the rigid diphenyl groups. Our long period values for PEEK agree reasonably well with the ones reported by other authors[8,12] while the lamellar thickness values are about 15% smaller than their values. This discrepancy could be attributed to the different experimental methods and the different models by which the structure parameters were deduced. It should be noted that both PEEK and D-PEEK revealed a lower lamellar thickness than expected when compared with some other semicrystalling polymers such as PET ($d \simeq$ 6–7 nm). The observations imply that PEEKs probably have low surface free energy. Together with high chain rigidity, the melting entropy is significantly reduced. The uncertainty of the above parameter values arises mainly from model assumption, whereas the data analysis errors, such as those from the extrapolation of data points at both small q and large q values for the Fourier transform, are only secondary in nature.

B. Crystallization Kinetics. The isothermal crystallization of PEEK has been found[8] to display a maximum rate at ~230 °C. About 50° below or above 230 °C, the isothermal crystallization becomes slow and has been analyzed by using the Avrami equation[23,32]

$$X_c(t)/X_c(\infty) = 1 - \exp(-kt^n) \tag{10}$$

where $X_c(t)$ and $X_c(\infty)$ are the crystallinity at time t and at the end of crystallization, respectively. The time t should be counted from the time when samples have reached the crystallization temperature T_c but without notable crystallization. The exponents, n and k, are the Avrami parameters which depend on the nucleation and the crystal growth mechanism. Theoretically, if the spherulitic crystalline state starts growing simultaneously, the value n should be 3, while if nucleation takes place sporadically in time and space, the n would be expected to be 4.[55] The exponent n has been reported to vary somewhere between 3 and 4, depending on the sample history for those slow isothermal crystallizations of PEEK.[23,32] Therefore, it has been believed that PEEK crystallizes heterogeneously by simultaneous nucleation

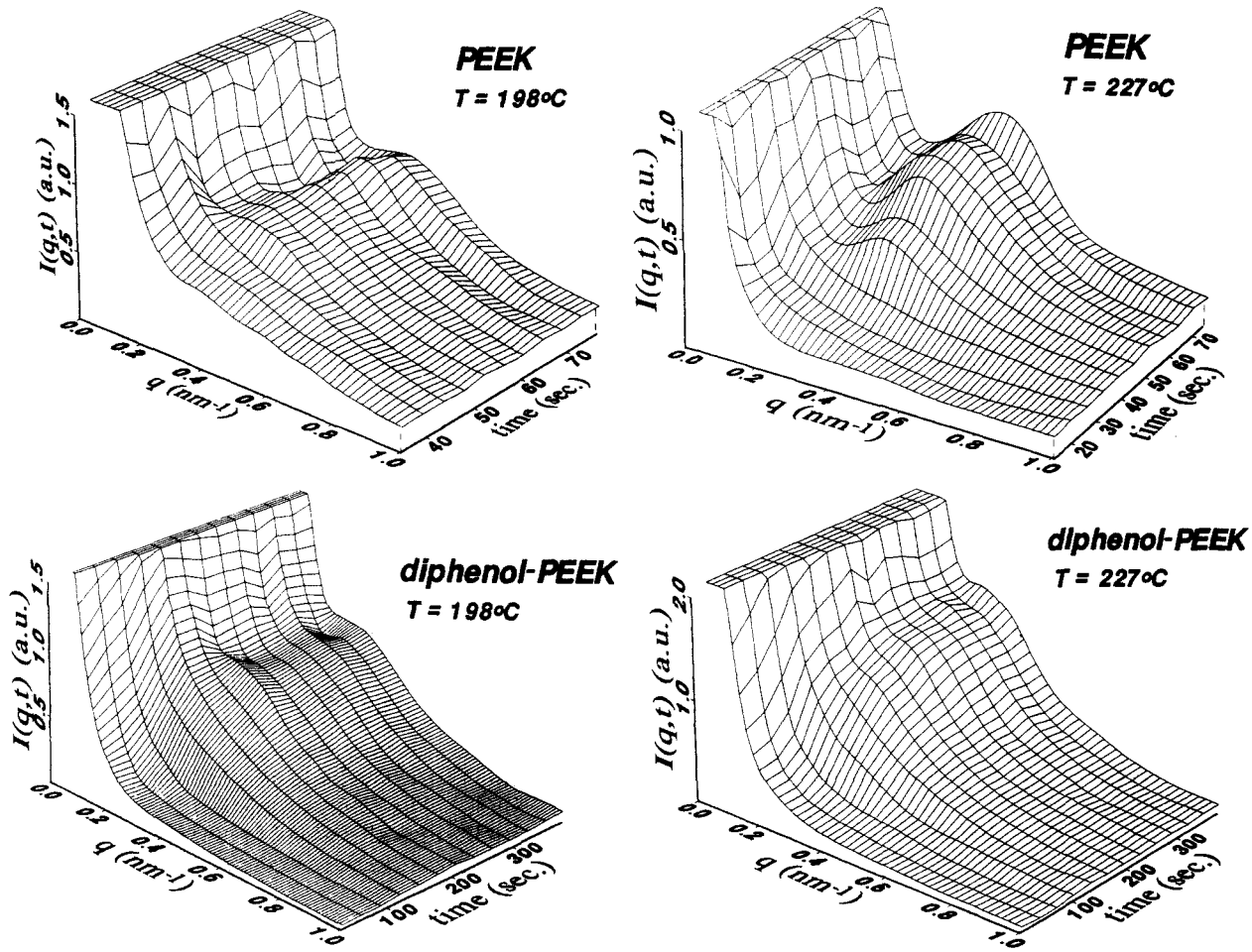

Figure 7. Time evolution of SAXS patterns after a temperature-jump from 50 °C to higher temperatures, which are indicated on the plot, for PEEK and D-PEEK from the amorphous state. The elapsed time was counted right after the sample was jumped into a high temperature chamber from a low temperature chamber. Fifty or more consecutive patterns were recorded from each sample with different accumulation time, t_a, and delay time, t_d, between two patterns: (a, top left) t_a = 3 s, t_d = 0 s; (b, top right) t_a = 3 s, t_d = 0 s; (c, bottom left) t_a = 10 s, t_d = 15 s; (d, bottom right) t_a = 10 s, t_d = 10 s. For each sample, some initial and later stage patterns which display no significant change are not presented here for a better view. All the patterns were smoothed as described in Figure 1.

due to the residual nucleating agent. In order to more explicitly compare the crystallization kinetics between PEEK and D-PEEK, we chose an extreme isothermal condition near 230 °C where the fastest crystallization might take place. Time-resolved SAXS profiles were collected during the isothermal crystallization by taking advantage of the high-flux synchrotron beam and the dual-chambered temperature jumper. The quenched amorphous samples were held in the side chamber (where T = 50 °C) of the temperature jumper for 5 min and then quickly inserted into the central chamber (where T was equal to the temperature (T_c) at which crystallization process was measured) of the temperature jumper, and right at that moment the time t was counted with 50 consecutive profiles being recorded in the time course. A minimum time interval of 3 s for each profile was set in the case of PEEK. Figure 7 illustrates a three-dimensional SAXS pattern following the crystallization kinetics of PEEK and D-PEEK. All the SAXS patterns presented here were smoothed using a points-add-up method and the cubic spline smoothing technique. In the initial stage in each set of patterns, one can see only the exponential-like decay curves without a notable peak associated with the periodic electron density fluctuations. With a further increase in time, a maximum at $q \sim 0.4$ nm^{-1} appears and becomes more pronounced and finally pertains no remarkable change.

The long periods estimated from the position of the maximum in the SAXS patterns using the previously mentioned method during the crystallization are plotted in Figure 8 for both PEEK and D-PEEK. Clearly, the long period for D-PEEK is larger than that for PEEK during the whole time course of isothermal crystallization. In the case of PEEK, the long period tends to decrease within 60 s of elapsed time and then shows a stable value. A possible reason for the decrease in the long period at the initial stage might be that the isothermal condition was not fulfilled within a short time as a result of the ramp of

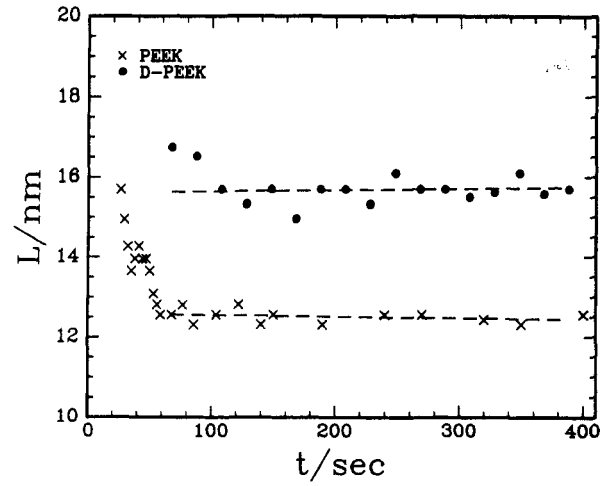

Figure 8. Long period of lamella structure for PEEK and D-PEEK as a function of time at 227 °C.

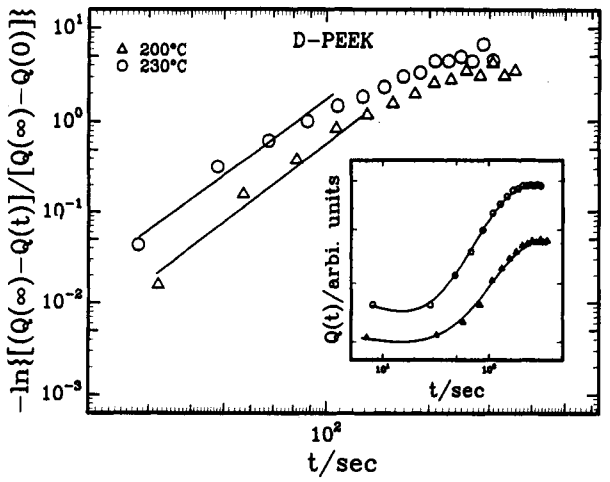

Figure 9. Avrami log–log plot of $-\ln\{[Q(\infty) - Q(t)]/[Q(\infty) - Q(0)]\}$ versus t for D-PEEK after a T-jump from 50 °C to the temperatures as marked on the plot. Solid lines represent the best fitting of initial linear section, yielding the Avrami parameters in eq 10 $n = 2.74$ and $k = 5.62 \times 10^{-6}$ s^{-1} at 227 °C and $n = 2.87$ and $k = 1.06 \times 10^{-6}$ s^{-1} at 198 °C. The inset is the corresponding time dependence of the invariant with the symbols having the identical meanings, showing no manifested change in the invariant before ~30 s. The solid curves in the inset are for guiding the eyes.

sample temperature. Nevertheless, we are not able to rule out other possibilities at the present time. For example, the crystal lamellae could be strongly corrugated during the early stage of crystallization and are flattened later on, as was postulated to explain the decrease of long period with time for PET.[56] In the case of D-PEEK, the long period displays no appreciable change with time.

It seems to be very important to calibrate the temperature response of the sample after the T-jump for the very fast isothermal crystallization because of the existence of a temperature retardation time by which the nonisothermal crystallization has already been taken place. For this purpose, the sample cell was filled with an epoxy thermosetting resin and a tiny thermocouple. The sample cell temperature was recorded at ~2-s intervals until it reached the chamber temperature. As observed by other authors,[57] the temperature change was exponential and could be described by

$$T(t) = T_c - (T_c - T_i)\exp(-t/t_0) \tag{11}$$

where $T(t)$ is the temperature at time t after T-jump from an initial temperature T_i to a crystallization temperature T_c. t_0 is the retardation time and was found to be 30.7 and 33.6 s for the T-jump from 50 to 227 °C and from 50 to 198 °C, respectively. The half time $t_{1/2}$, which is the time by which half of the change of Q has taken place, was found to be 31 and 29 s for PEEK at, respectively, 198 and 227 °C, and 101 and 73 s for D-PEEK at, respectively, 198 and 227 °C. The slower crystallization rate for D-PEEK represents the additional difficulty in molecular rearrangement and repacking of crystalline structure elements created by the diphenyl groups during crystallization. It is apparent that the crystallization for PEEK at 198 and 227 °C in our T-jump experiment is not an ideal isothermal process as a consequence of the temperature retardation and therefore cannot be treated by an Avrami type analysis. In the case of D-PEEK, since the crystallization process was slower and the main crystallization could be approximately considered as an isothermal process, the Avrami analysis was performed as shown in Figure 9, the inset showing the plot of the invariant Q versus the time t. The quantity $[Q(\infty) - Q(t)]/[Q(\infty) - Q(0)]$ depicts the relative change of the invariant, which is proportional to $X_c(1 - X_c)$ provided that the electron density difference $\Delta\rho$ between the crystalline and the amorphous regions remains constant during the isothermal crystallization. It was found[58] that the $\Delta\rho$ was indeed almost constant during the isothermal crystallization for a similar semicrystalline polymer. If we assume a constant $\Delta\rho$, the observed increase in Q corresponds purely to an increase in the product of X_c and $(1 - X_c)$. In the main part of Figure 9, a fitting of the initial linear portion of the curves before the roll-off yielded the Avrami parameters $n = 2.74$ and $k = 5.62 \times 10^{-6}$ s^{-1} at 227 °C and $n = 2.87$ and $k = 1.06 \times 10^{-6}$ s^{-1} at 198 °C. The n values close to 3 are supposed to imply that the nucleation takes place simultaneously and the crystal grows spherulitically. However, this fitting does not seem to be quite convincing since the points above ~100 s deviate remarkably from the linear fitting curve and the values of the fitting parameters vary largely depending on the fitting range. The problem might be at least partially due to the fact that several assumptions in the Avrami analysis method are not pertinent to complicated polymer crystallizations.[55] Also, the invariant change reflects the change of a product, $X_c(1 - X_c)$, rather than X_c itself.

For a fast polymer isothermal crystallization, if the nucleation takes place simultaneously within a negligible time scale, the crystallization rate could be dominated by a molecular diffusion mechanism. Under such a condition, the invariant change during the isothermal crystallization process, analogous to the order–disorder transition process,[59] might be characterized by a relaxation time τ

$$Q(t) = Q(\infty) - [Q(\infty) - Q(0)]\exp\left(-\frac{t}{\tau(T)}\right) \tag{12}$$

This equation was derived by Hashimoto[59] from the time-dependent Ginzburg–Landau theory,[60] a diffusion equation of the Langevin type. In a nonideal T-jump process, the retarded temperature response from the sample could manifest a substantial effect on the scattered intensity. A multistep T-jump process can be employed to correct this effect after knowing the relationship of temperature response with time. This approach divides evenly the whole time period into N intervals of Δt ($=t_{j+1} - t_j$). At time t_j, the temperature is T_j. Assuming that each T-jump from T_j to T_{j+1} at time t_{j+1} occurs ideally, then we have

$$Q(t_{j+1}) = Q(\infty) - [Q(\infty) - Q(t_j)]\exp\left(-\frac{\Delta t}{\tau(T_j)}\right) \tag{13}$$

where the running index j goes from 1 to $N - 1$ with $T_1 = T_i$ (initial temperature) and $T_N = T_c$ (crystallization temperature). Equation 13 can be rewritten as

$$Q(t_N) = Q(\infty) - [Q(\infty) - Q(t_1)]\exp\left(-\Delta t\sum_{j=1}^{N-1}\frac{1}{\tau(T_j)}\right) \tag{14}$$

If the temperature dependence of $\tau(T_j)$ is known, one can estimate $Q(t)$. In this work the relaxation time $\tau(T)$ was assumed to follow the general form[61]

$$\tau(T) = \tau_0\exp\left(\frac{\Delta H}{RT}\right) \tag{15}$$

where ΔH is the activation energy of segmental motion and τ_0 is the pre-exponential factor.

Figure 10 shows the half-log plots (open symbols) of $[Q(\infty) - Q(t)]/[Q(\infty) - Q(0)]$ versus t for (a) PEEK and (b) D-PEEK at the crystallization temperatures 198 and 227 °C. The initial decay with time is nonexponential but becomes exponential after the time t is much larger than temperature retardation time t_0 in eq 11. The solid lines

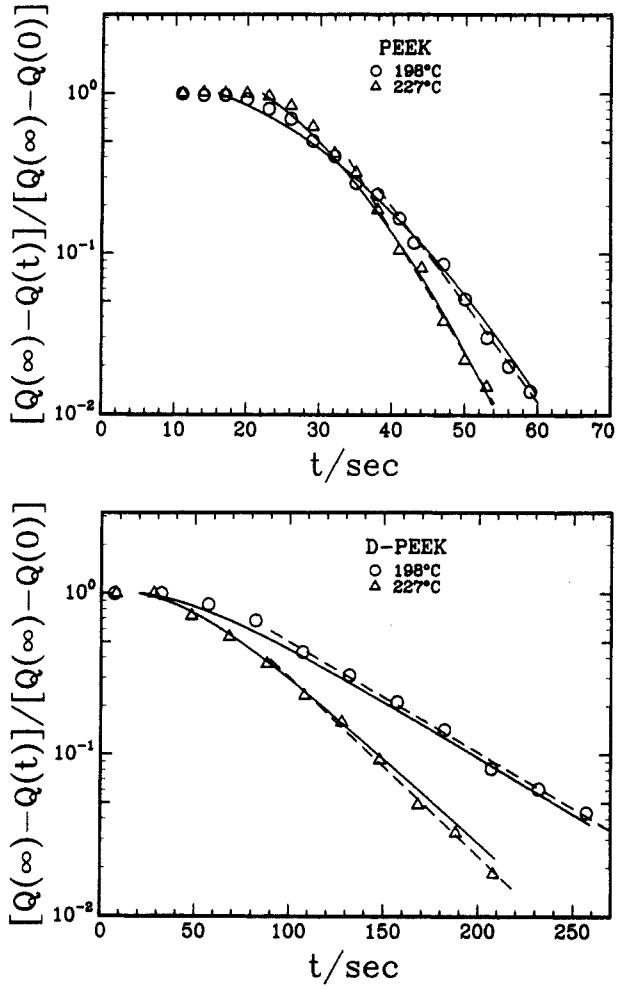

Figure 10. Half-log plot of $[Q(\infty) - Q(t)]/[Q(\infty) - Q(0)]$ versus t for PEEK and D-PEEK. The open symbols represent the experimental points and the solid lines represent the best fit by using eqs 14, 15, and 11. The fitting parameters of activation energy, ΔH, and pre-exponential factor, τ_0, are ΔH = 7.6 kcal/mol and $\tau_0 = 2.7 \times 10^{-3}$ s for PEEK at 198 °C, ΔH = 8.3 kcal/mol and $\tau_0 = 1.5 \times 10^{-3}$ s for PEEK at 227 °C, ΔH = 9.6 kcal/mol and $\tau_0 = 5.0 \times 10^{-3}$ s for D-PEEK at 198 °C, and ΔH = 9.4 kcal/mol and $\tau_0 = 6.8 \times 10^{-3}$ s for D-PEEK at 227 °C. The broken lines represent the linear square fitting curves for the data points at the time scale larger than the retardation time of the temperature response of the sample. The relaxation time τ for the diffusion-controlled crystallization process estimated from the slope of the linear fitting curves are 7.2 s.

represent the best fitting curves by using eqs 14, 15, and 11 with two fitting parameters τ_0 and ΔH. The fitting was accomplished using the Levenberg–Marquardt algorithm, yielding an activation energy ΔH between 7.6 and 8.3 kcal/mol for PEEK and between 9.4 and 9.6 kcal/mol for D-PEEK, and a pre-exponential factor τ_0 to be of the order of 1.5×10^{-3} to 2.7×10^{-3} s for PEEK and 5.0×10^{-3} to 6.8×10^{-3} s for D-PEEK. By comparing the two parameters between PEEK and D-PEEK, one can see that the ΔH for D-PEEK is ~10% larger than that for PEEK and the τ_0 for D-PEEK is several-fold larger than that for PEEK. It is noted from Figure 10 that the T-jump process becomes ideal at $t \gg t_0$, displaying straight lines in accordance with eq 12. From the slope of the linear section of the curves, as shown by the broken lines, the relaxation time τ was estimated to be 7.2 and 5.7 s for PEEK at, respectively, 198 and 227 °C, and 63 and 39 s for D-PEEK at, respectively, 198 and 227 °C. It should be stressed that the application of the single exponential equation to the very fast isothermal crystallization process in this work can only be viewed as a semiquantitative analysis as the assumption that nucleation stage is negligible may not be valid for the system. However, as a first-order approximation, the crystal growth under our particular conditions seems to be mainly controlled by a diffusion coefficient of segmental elements. With a further increase in temperature, the diffusion mechanism may play only a secondary role due to the outstanding melting or rearrangement of the lamellar structures by the rubbery elastic force, resulting in a slower crystallization process.

Conclusions

SAXS profiles for PEEK and D-PEEK have shown a strong temperature dependence. With increasing temperature, the position of the maximum associated with the long period shifts toward smaller angles and the integrated area under the profile or the invariant Q associated with the crystallinity increases before melting. One-dimensional correlation functions of electron density fluctuations deduced from the SAXS profiles by using the inverse Fourier transform technique have provided the long periods which are in agreement with those obtained by applying the Bragg equation to the maximum in the Lorentz corrected SAXS profiles. D-PEEK displays a larger long period, a smaller lamellar thickness, and a lower crystallinity than those for PEEK over a wide temperature range we studied. The long period for PEEK was found to increase from 10.1 to 16.9 nm with increasing temperature from 170 to 330 °C while the lamellar thickness was found to increase from 2.3 to 5.0 nm at the same time. D-PEEK showed a similar trend. This evidence seems to support the two-morphology explanation for the double-melting behavior for most semicrystalline polymers. The larger ratio of the amorphous layer thickness to the lamellar thickness for D-PEEK as compared to that for PEEK has proved the more restricted mobility of diphenyl groups in the amorphous region.

The isothermal crystallization in a temperature jump process from the glassy state for PEEK and D-PEEK was very fast with a half time, $t_{1/2}$, of 31 and 101 s, respectively, for PEEK and D-PEEK at 198 °C and of 29 and 73 s, respectively, for PEEK and D-PEEK at 227 °C. The time evolution of the invariant during the fast isothermal crystallization did not seem to follow the Avrami equation well. An exponential behavior was observed; i.e., the fast isothermal crystallizations appeared to be diffusion-controlled processes and the nucleation stage was of secondary importance. The initial nonisothermal condition during the temperature jump could be corrected by using a multistep T-jump procedure. The best fitting of these nonisothermal data yielded an average activation energy ΔH to be of the order of 8.0 and 9.5 kcal/mol for PEEK and for D-PEEK, respectively.

Acknowledgment. B.C. greatly acknowledges the Polymers Program, National Science Foundation (DMR-8921968), the U.S. Army Research Office (DAAL-0391G0040), and the U.S. Department of Energy (DEFG-0286ER45237A005 and DEFG0589ER75515) for the support of this research as well as the Alexander von Humboldt Foundation for the continuation of his Humboldt award for senior U.S. scientists. M.A. acknowledges the Dirección General de Investigación Científica y Técnica of Spain which is supporting her stay at the State University of New York at Stony Brook with a grant of the Programa Nacional de Formación del Personal Investigador. The authors appreciate the helpful suggestions made by the reviewers.

References and Notes

(1) Lustiger, A. *SAMPE J.* **1984**, Sept/Oct, 26.
(2) Jones, D. P.; Leach, D. C.; Moore, D. R. *Polymer* **1985**, *26*, 1385.
(3) Seferis, J. C. *Polym. Comput.* **1986**, *7*, 158.
(4) Wu, Z.; Zheng, Y. B.; Yu, H. Z.; Seki, M.; Yosomiya, R. *Angew. Makromol. Chem.* **1988**, *164*, 21.
(5) Hsaio, B. S.; Chen, E. J. H. *Proc. Mater. Res. Soc. Symp.* **1990**, 170.
(6) Mullins, M. J.; Woo, E. P. *J. Macromol. Sci. Macromol. Chem. Phys.* **1987**, *27*, 313.
(7) Rueda, D. R.; Ania, F.; Richardson, A.; Ward, I. M.; Balta-Calleja, F. *J. Polym. Commun.* **1983**, *24*, 258.
(8) Blundell, D. J.; Osborn, B. N. *Polymer* **1983**, *24*, 953.
(9) Wakelyn, N. T. *Polym. Commun.* **1984**, *25*, 306.
(10) Hay, J. N.; Kemmish, D. J.; Langford, J. I.; Rae, A. I. M. *Polym. Commun.* **1984**, *25*, 175.
(11) Hay, J. N.; Kemmish, D. J.; Langford, J. I.; Rae, A. I. M. *Polym. Commun.* **1985**, *26*, 283.
(12) Yoda, O. *Polym. Commun.* **1985**, *26*, 16.
(13) Frantini, A. V.; Cross, E. M.; Whitaker, R. B.; Adams, W. W. *Polymer* **1986**, *27*, 861.
(14) Wakelyn, N. T. *J. Polym. Sci. Polym. Lett.* **1987**, *25*, 25.
(15) Hay, J. N.; Kemmish, D. J.; Lloyd, J. R. *Polymer* **1989**, *30*, 489.
(16) Hay, J. N.; Kemmish, D. J. *Polym. Commun.* **1989**, *30*, 77.
(17) Kemmish, D. J.; Hay, J. N. *Polymer* **1985**, *26*, 905.
(18) Lee, Y.; Porter, R. S. *Polym. Eng. Sci.* **1986**, *26*, 633.
(19) Valinaris, C. N.; Seferis, J. C. *Polym. Eng. Sci.* **1986**, *26*, 1674.
(20) Cheng, S. Z. D.; Wunderlich, B. *J. Polym. Sci. Polym. Phys. Ed.* **1986**, *27*, 1755.
(21) Cheng, S. Z. D.; Cao, M. Y.; Wunderlich, B. *Macromolecules* **1986**, *19*, 1868.
(22) Jog, J. F.; Nakkarni, V. M. *J. Appl. Polym. Sci.* **1986**, *32*, 3317.
(23) Cebe, C. R.; Hong, S. D. *Polymer* **1986**, *27*, 1183.
(24) Blundell, D. J. *Polymer* **1987**, *28*, 2248.
(25) Lee, Y.; Porter, R. S. *Macromolecules* **1987**, *20*, 1336.
(26) Chang, S. Z. D.; Linn, S.; Judovits, L. H.; Wunderlich, B. *Polymer* **1987**, *28*, 10.
(27) Ostberg, G. M. K.; Seferis, J. C. *J. Appl. Polym. Sci.* **1987**, *33*, 29.
(28) Bassett, D. C.; Olley, R. J.; Al Raheil, I. A. M. *Polymer* **1988**, *29*, 1745.
(29) Cebe, P. *J. Mater. Sci.* **1988**, *23*, 3721.
(30) Cebe, P. *Polym. Eng. Sci.* **1988**, *28*, 1192.
(31) Cebe, P. *Polym. Compos.* **1988**, *9*, 271.
(32) Lee, Y.; Porter, R. S. *Macromolecules* **1988**, *21*, 2770.
(33) Chang, S. S. *Polym. Commun.* **1988**, *29*, 138.
(34) Mingbi, Q.; Xiasnan, X.; Jun, Z.; Wei, W.; Zongneng, Q. *Thermochim. Acta* **1988**, *134*, 223.
(35) Day, M.; Suprunchuk, T.; Cooney, J. D.; Wiles, D. M. *J. Appl. Polym. Sci.* **1988**, *36*, 1097.
(36) Choe, C. R.; Lee, K. H. *Polym. Eng. Sci.* **1989**, *29*, 801.
(37) Khanna, Y. P.; Kumar, R. *J. Polym. Sci. Polym. Phys. Ed.* **1989**, *27*, 369.
(38) Kenny, J.; D'Amore, A.; Nicolais, L.; Iannone, M.; Scatteia, B. *SAMPE J.* **1989**, *25*, 27.
(39) Day, M.; Deslandes, Y.; Roovers, J.; Suprunchuk, T. *Polymer* **1991**, *32*, 1258.
(40) Lovinger, A. J.; Davis, D. D. *Macromolecules* **1986**, *19*, 1861. Lovinger, A. J.; Hudson, S. D.; Davis, D. D. *Macromolecules* **1992**, *25*, 1752. Hudson, S. D.; Davis, D. D.; Lovinger, A. J. *Macromolecules* **1992**, *25*, 1759 (PEEK/poly(ether imide) blends).
(41) Kumar, S.; Anderson, D. P.; Adams, W. *Polymer* **1986**, *27*, 329.
(42) Deslandes, Y.; Sabir, F.; Roovers, J. *Polymer* **1991**, *32*, 1267.
(43) Wu, Z.; Zhang, J.; Yosomiya, R. To be submitted for publication.
(44) Hsiao, B. S.; Gardner, K. H.; Wu, D.; Chu, B. *Polym. Prepr.* **1992**, *33* (1), 265.
(45) Chu, B.; Wu, D.; Wu, C. *Rev. Sci. Instrum.* **1987**, *58*, 1158.
(46) Chu, B.; Wu, D.; Howard, R. L. *Rev. Sci. Instrum.* **1989**, *60*, 3224.
(47) Glatter, O., Kratky, O., Eds.; *Small Angle X-ray Scattering*; Academic Press: London, 1982.
(48) Strobl, G. R.; Schneider, M. *J. Polym. Sci., Polym. Phys. Ed.* **1980**, *18*, 1343.
(49) Debye, P.; Bueche, A. M. *J. Appl. Phys.* **1949**, *20*, 518.
(50) Debye, P.; Anderson, H. R., Jr.; Brumberger, H. *J. Appl. Phys.* **1957**, *28*, 679.
(51) Ruland, W. J. *J. Appl. Crystallogr.* **1971**, *4*, 70.
(52) Vonk, C. G.; Kortleve, G. *Kolloid-Z.* **1967**, *220*, 19.
(53) Strobl, G. R.; Schneider, M. *J. Polym. Sci., Polym. Phys. Ed.* **1980**, *18*, 1343.
(54) Cruz, C. S.; Stribeck, N.; Zachmann, J. G. *Macromolecules* **1991**, *24*, 5980.
(55) Wunderlich, B. *Macromolecular Physics*; Academic Press: New York, 1977; Vol. 2.
(56) Elsner, G.; Zachmann, H. G.; Milch, J. R. *Makromol. Chem.* **1981**, *182*, 657.
(57) Hashimoto, T.; Kowsaka, K.; Shibayama, M.; Suehiro, S. *Macromolecules* **1986**, *19*, 750.
(58) Gehrke, R. *Topics in Current Chemistry*; Springer: Berlin, 1989; Vol. 151.
(59) Hashimoto, T. *Macromolecules* **1987**, *20*, 465.
(60) Gunton, J. D.; San Miguel, M.; Sahni, P. S. *Phase Transitions and Critical Phenomena*; Domb, C., Lebowitz, J. L., Eds.; Academic Press: New York, 1983; Vol. 8.
(61) Bartenev, G. M., Zelenev, Yu. V., Eds. *Relaxation Phenomena in Polymers*; John Wiley & Sons: New York, 1974.

Registry No. PEEK, 31694-16-3; ((*p*-FC_6H_4)$_2$CO)(*p*-HOC_6H_4-OH) (copolymer), 29658-26-2; (*p*-$HOC_6H_4C_6H_4$-*p*-OH)((*p*-FC_6H_4)$_2$-CO)(*p*-HOC_6H_4OH) (copolymer), 104570-14-1.